A Strategy for Enhancing Ultrahigh Molecular Weight Block Copolymer Chain Mobility to Access Large Period Sizes (> 100 nm)

Cian Cummins,[†,‡,*] Alberto Alvarez-Fernandez,[§] Ahmed Bentaleb,[†] Georges Hadziioannou,[‡] Virginie Ponsinet,[†*] and Guillaume Fleury[‡*]

[†]CNRS, Univ. Bordeaux, Centre de Recherche Paul Pascal, UMR 5031, 115 Avenue Schweitzer, 33600 Pessac, France.
[‡]Univ. Bordeaux, CNRS, Bordeaux INP, LCPO, UMR 5629, F-33600, Pessac, France.
[§]Department of Chemical Engineering, University College London, Torrington Place, London WC1E 7JE, U.K.

Keywords: Block copolymers; large period patterning; surface chemistry; metasurfaces; optical nanoresonators.

ABSTRACT:

Assembling ultra-high molecular weight (UHMW) block copolymers (BCPs) in rapid timescales is perceived as a grand challenge in polymer science due to slow kinetics. Through surface engineering and identifying a non-volatile solvent (propylene glycol methyl ether acetate, PGMEA) we showcase the impressive ability of a series of lamellar poly(styrene)-*block*-poly(2-vinylpyridine) (PS-*b*-P2VP) BCPs to self-assemble directly after spin-coating. In particular, we show the formation of large period (≈ 111 nm) lamellar structures from a neat UHMW PS-*b*-P2VP BCP. The significant influence of solvent-polymer solubility parameters are explored to enhance polymer chain mobility. After optimization using solvent vapor annealing, increased feature order of ultra large period PS-*b*-P2VP BCP patterns in 1 hr is achieved. The methods described in this article center on industry compatible patterning schemes, solvents and deposition techniques. Isolated metallic and dielectric features are also demonstrated exemplifying the promise that large BCP periods offer for functional applications. Thus, our straightforward

UHMW BCP strategy potentially paves a viable and practical path forward for large-scale integration in various sectors, *e.g.* photonic band gaps, polarizers, and membranes that demand ultra large period sizes.

INTRODUCTION:

The chemically incompatible configuration of block copolymers (BCPs) can induce microphase separated structures that provides a versatile platform for thin film applications. Precise engineering of molecular block architecture can form BCP thin films with spherical, cylindrical, gyroidal and lamellar geometries.[1,2] Resultant BCP geometries are related to respective block volume fractions (*f*) and overall degree of polymerization (N) can be modified to produce feature sizes and periods predominantly from 10 nm up to 50 nm.[3] The inherent ability of BCP thin films to define these nanoscale geometries has enabled the templating of materials for membrane, photonic, nanoeletronic, and biological applications amongst others.[4,5,6,7,8,9,10,11,12,13,14] Whilst BCPs typically constitute organic based blocks, an individual block can be selectively modified to produce inorganic nanofeatures through vapor, vacuum or solution based deposition processes.[15] This facet of BCP materials has led to the generation of nanofeatures including Fe_3O_4 nanodots for hydrogen peroxide sensing,[16] Au/Pt structures as memory devices,[17] WO_3 nanowires as active device channels,[18] and TiO_2 layers for perovskite solar cells.[19]

Recently, there has been a growing interest examining the use of ultra-high molecular weight (UHMW) BCPs to fabricate features and periods above 100 nm. Patterning above 100 nm potentially opens up an attractive and cheap route to functional surfaces for areas such as photonics[20,21,22] to move beyond the cumbersome and expensive top-down lithography used hitherto. However, the kinetic barriers associated with polymer chain

entanglement of UHMW linear BCPs thereby slowing self-assembly is recognized as a grand challenge. To date, bottlebrush polymers have been more appealing due to faster associated kinetic pathways for self-assembly in contrary to their linear BCP counterparts.[23,24] Thus, studies on UHMW BCP thin film self-assembly are scarce, with only four studies (to the best of our knowledge) reported on lamellar BCP systems. Yang *et al.* demonstrated the use of a lamellar poly(styrene)-*block*-poly(2-vinylpyridine) (PS-*b*-P2VP) system (Mw = 265 kg mol^{-1}) to form feature sizes greater than 100 nm.[25] However, various issues contributed to poor PS-*b*-P2VP film formation and lengthy solvent vapor anneal periods were required, *e.g.* from 2 to 48 hrs. The other UHMW reports have used PS-*b*-poly(methyl methacrylate) (PS-*b*-PMMA) BCP materials and a combinatorial approach to induce self-assembly and improve pattern ordering. In the first case, Kim *et al.* demonstrated periods of ≈ 200 nm for a lamellar PS-*b*-PMMA (Mw = 1000 kg mol^{-1}) BCP using a 10 hr solvent vapor anneal (tetrahydrofuran) treatment followed by a 3 hr thermal anneal process.[26] Doerk *et al.* introduced so-called "smart solvents" whereby they used PS and PMMA homopolymers blended in UHMW PS-*b*-PMMA BCPs (Mw = 1051 kg mol^{-1} and 2000 kg mol^{-1} respectively) to pattern periods close to 211 nm.[27] Their process is markedly shorter, using only 1 hr for solvent vapor annealing (tetrahydrofuran) and 5 mins for thermal annealing. Additionally, excellent pattern transferred silicon nanostructures were realized after converting PMMA materials to AlOx nanowires using sequential infiltration synthesis. Lastly, in 2020, Hayashi and co-workers reported the real time self-assembly observation of an UHMW PS-*b*-PMMA (Mw = 1010 kg mol^{-1}).[28] While ≈ 180 nm period lamellar features were achieved, very long solvent vapor annealing times (6 to 8 hrs) were required, which is problematic from a fabrication standpoint. Others have also demonstrated large period cylindrical

patterns;[29,30] however, robust routes that use compatible solvents and truly rapid deposition methods do not exist for assembling UHMW BCPs.

Here, we outline a strategy that exemplifies the attention required for solvent choice to enhance polymer chain mobility of lamellar PS-*b*-P2VP BCPs. To this end, our process is centrally based upon spin coating of PS-*b*-P2VP thin films from a non-volatile solvent (propylene glycol methyl ether acetate, PGMEA). In particular, the self-assembly of a UHMW PS-*b*-P2VP lamellar BCP possessing ≈ 111 nm period has been elucidated with surface pre-treatment and solvent vapor annealing of the PS-*b*-P2VP films in 1 hr. The ability to form such ordered large period structures is intrinsically linked to solvent choice, control of the polymer/substrate and polymer/air interfaces that have been rigorously investigated. Overall, the methodology presented in this article provides insight into a versatile method of attaining ultra-large periodic gratings in a low cost, rapid, and scalable process via a UHMW PS-*b*-P2VP BCP.

EXPERIMENTAL:

Materials

Planar Si substrates (from Si-Mat silicon materials) used were highly polished single-crystal silicon <100> wafers (p-type) with a native oxide layer of ≈2 nm. Poly(styrene)-*stat*-poly(methyl methacrylate) (PS-*stat*-PMMA) copolymer (f_{PS} = 0.63) was provided by ARKEMA. A random copolymer of poly(styrene)-*stat*-poly(2-vinylpyridine) with a Mn = 71 kg mol^{-1}) and three poly(styrene)-*block*-poly(2-vinylpyridine) (PS-*b*-P2VP) (referred to as PSPVP1, PSPVP2, and PSPVP3 respectively from herein) BCPs with a molecular weight of Mn = 429 kg mol^{-1} (M_{nPS} = 213 kg mol^{-1} ; M_{nP2VP} = 215 kg mol^{-1}), Mn = 199 kg mol^{-1} (M_{nPS} = 102 kg mol^{-1} ; M_{nP2VP} = 97 kg mol^{-1}), and Mn = 50 kg mol^{-1}

(M_{nPS} = 25 kg mol^{-1} ; M_{nP2VP} = 25 kg mol^{-1}) were purchased from Polymer Source, Inc., Canada and were used without further purification. See table 1 below for all polymer material characteristics provided by supplier and details of deposition conditions. Propylene glycol methyl ether acetate (PGMEA) (Reagent Plus, 99.5%), toluene (Reagent Plus, 99.5%), chloroform (Reagent Plus, 99.5%), and acid tetrachloroauric ($HAuCl_4$) (99.999% trace metals basis) were purchased from Merck.

Surface Functionalization and Block Copolymer Film Preparation

Three different surface treatments were studied for PSPVP1-3 BCPs. Please note that a fourth surface treatment was required to enhance PSPVP3 ordering, as detailed below. Firstly, silicon wafers were cleaned solely in solvent (toluene, chloroform or PGMEA was used depending on deposition solvent). Secondly, silicon wafers rinsed in organic solvent were treated with UV/O_3 for 10 mins. The final baseline treatment studied for PSPVP1-3 used silicon wafers coated with 2.0 wt. % PGMEA solution of poly(styrene)-*stat*-poly(methyl methacrylate) (PS-*stat*-PMMA) copolymer (f_{PS} = 0.63) with a subsequent thermal anneal at 230°C for 5 minutes to promote grafting. Grafting of random copolymer brushes to solid substrates is a highly useful strategy in the BCP community to balance substrate surface energies and thereby control BCP microdomain orientation and pattern coverage.[31] In our work, we have attached brushes to silicon substrates via the "grafting to" process, achieved through condensation reactions.[32] After baking, rinsing of ungrafted polymer material was carried out using PGMEA. PSPVP1-3 BCP solutions were dissolved in PGMEA, (or toluene or chloroform) and left stirring until fully dissolved. 0.85 µL of respective solutions were then deposited on modified silicon wafers at 2000 rpm for 30 secs. For enhanced ordering of PSPVP3, a PS-*stat*-P2VP surface treatment was employed. We used a Si surface functionalized with a 0.5 wt

% PS-*stat*-P2VP in PGMEA. PS-*stat*-P2VP films were deposited at 2000 rpm for 30 secs and baked at 190°C for 10 mins. Rinsing of the excess PS-*stat*-P2VP material was carried out with PGMEA. After deposition of PSPVP3, static solvent vapor annealing[33] in a glass jar (total volume 50 cm^3) with a PGMEA/chloroform (3:1) atmosphere was carried out for up to 1 hr at room temperature (20°C).

Table 1. Polymers used for substrate surface modification, lamellar PS-*b*-P2VP BCP material characteristics and deposition conditions used in this study.

Polymer	Total Mn (kg mol^{-1})	χN	PDI	Solution conc. (%)	Film thickness (nm)	Period (nm)
PS-*stat*-PMMA	12	-	1.4	2	-	-
PS-*stat*-P2VP	71	-	1.6	0.5	-	-
PSPVP1	50	85	1.5	1.5	≈ 40-45	≈ 30
PSPVP2	199	338	1.15	1.0	≈ 35-40	≈ 64
PSPVP3	428	728	1.29	1.5	≈ 45-50	≈ 111

Au Pattern Formation

Microphase separated PSPVP patterns were converted to Au replicas using $HAuCl_4$. Varying concentrations (*i.e.* 1, 5, and 10 wt. % *aq.* solution) of $HAuCl_4$ solutions were deposited on 2 × 2 cm^2 PSPVP patterns, and left for 60 seconds before spin coating at 2000 rpm for 30 secs to remove excess Au ion material. Films were subsequently treated in a plasma tool (PE-100 chamber) with O_2 plasma (20 sccm, 60W) for 60 seconds to remove the polymeric template and convert Au material to Au^0.

AlO_x Pattern Formation

Sequential infiltration synthesis (SIS). AlO_x was performed using an ALD (Ultratech SAVANNAH G2) tool in exposure mode. This mode allowed AlO_x SIS using an alternating exposure of P2FEMA based BCP thin films to trimethylaluminum (TMA) and

deionized water at 80°C with a purge under N_2 gas flow after each exposition. During exposure time, pressure in the ALD chamber increased leading to an infiltration of species in P2VP microdomains, then during purge time, unreacted precursor was removed by N_2 flow. Exposure and purge times used in this experiment were 60 and 300 s, respectively, for both precursors. Here we used three and five cycles (TMA/purge/H2O/purge) of SIS to form AlOx nanofeatures. Following SIS treatments, film were then plasma treated with O_2 plasma (40W, 3 mins, 20 sccm) to remove polymer and create AlOx features.

Characterization

Film morphology. AFM (Dimension Fast Scan, Bruker) was used in tapping mode to characterize the surface morphology of PSPVP1-3 BCPs and silicon cantilevers (Fastscan-A) with a nominal tip radius of 5 nm and a spring constant about 18 N m^{-1} were used. The resonance frequency of the cantilevers was about 1400 kHz. A JEOL 7800-E Prime SEM was used in super high-resolution gentle beam (GBSH) with an accelerating voltage of 1 kV. Dynamic light scattering (DLS) experiments at 25°C were performed on a Vasco 3 particle size analyzer from Cordouan equipped with a 40 mW diode laser operating at 658 nm. Three sub-runs of 60 s were recorded for each sample and the correlogram of each sub-run was analyzed by the 2^{nd} order cumulant method given access to particle mean sizes (hydrodynamic diameter, D_H) and distribution widths. Grazing incidence small angle X-ray scattering (GISAXS) experiments were performed at the Centre de Recherche Paul Pascal (CRPP) at Université de Bordeaux using a high resolution X-ray spectrometer Xeuss 2.0 from Xenoxs operating with radiation wavelength of λ = 1.54 Å. 2D scattering patterns were collected using a PILATUS 300K Dectris detector with a sample-to-detector distance of 1635 mm. The beam center position and the angular range were calibrated using a silver behenate standard sample. GISAXS

patterns were reduced using the GIXSGUI package,[34] where $q_y = 2\pi/\lambda\left[\sin(2\theta_f)\cos(\alpha_f)\right]$ and $q_z = 2\pi/\lambda\left[\sin(\alpha_f) + \sin(\alpha_i)\right]$ are the modulus of the scattering vectors in the direction parallel and perpendicular to the substrate plane and α_i, $2\theta_f$ and α_f are the incident and scattering angles in the horizontal and vertical directions, respectively.

Substrate surface chemistry. X-ray photoelectron spectroscopy (XPS) analyses were carried out using a Thermo Fisher Scientific K-Alpha spectrometer with a monochromatic Al Kα source (E = 1486.6 eV). The X-ray spot size was 200 mm. The spectrometer was calibrated with monocrystalline gold and silver foils. Survey spectra were acquired with a pass energy of 100 eV and high-resolution spectra were acquired with a pass energy of 20-40 eV. Thermo Scientific Avantage software was used for fitting and quantification. The optical study of the films deposited on silicon-wafers was performed using variable angle spectroscopic ellipsometry (VASE) in reflection with a phase modulated spectroscopic ellipsometer (UVISEL, from Horiba Scientific) on the spectral range [0.6–4.8 eV, *i.e.* 258–2000 nm]. We used the UVISEL II (A = 45º; M = 0º) configuration, where A and M denote the azimuthal orientations of the input polarizer and the photoelastic modulator, respectively, with respect to the plane of incidence. Three values of the incidence angle 50°, 60° and 70° were used and analyzed simultaneously. Surface free energy calculation of modified surfaces. Contact angle measurements were carried out on a Drop Shape Analyzer KRUSS DSA100S at 22ºC using 2µL drop of DI water, testing 3 different films in 3 different positions. PS-*stat*-PMMA and PS-*stat*-P2VP modified surfaces were analyzed in order to calculate surface free energy. Spin coating (2000 rpm, 30 secs) was carried out using 2 wt. % (PS-*stat*-PMMA) and 0.5 wt. % (PS-*stat*-P2VP) PGMEA solutions.

RESULTS & DISCUSSION:

As-cast UHMW PSPVP3 Pattern Formation: Effect of Deposition Solvent. The Flory interaction parameter (χ) between PS and P2VP has been reported as -0.033 + 63/T(K),[35] *i.e.* 0.178 at 25°C (273.15K). Values of χ_N are 85, 338, and 728 for PSPVP1, PSPVP2, and PSPVP3 BCPs respectively. Therefore, all PSPVP materials used here are in the strong segregation regime. **Figure 1** shows schematically the micellar and lamellar features observed experimentally depending on the use of toluene, chloroform, and PGMEA as the deposition solvent for PSPVP3 BCPs in as-cast films on UV/O_3 cleaned substrates. While micelles are commonly formed from PSPVP BCP materials in PS selective solvents like toluene,[36,37,38,39,40] as we moved towards more P2VP neutral solvents (polymer-solvent interaction values are discussed later) such as chloroform and PGMEA, the formation of ordered out-of-plane lamellar PS-*b*-P2VP features emerged for PSPVP3.

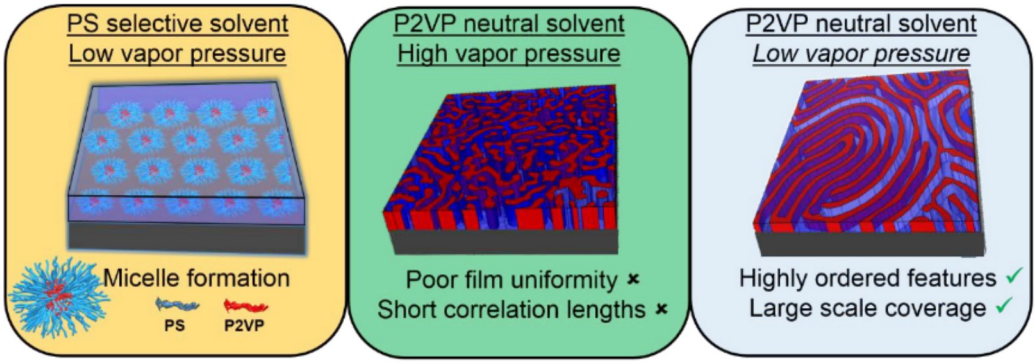

Figure 1. Scheme showing contrast between using a PS selective or P2VP neutral solvent and observed nanostructure formation for PS-*b*-P2VP BCPs in this study, in particular for PSPVP2 and UHMW PSPVP3. Note that PSPVP3 required solvent vapor annealing to enhance correlation lengths.

Figure 2 a-c displays corresponding AFM height images of PSPVP3 films cast from toluene, chloroform and PGMEA on UV/O_3 cleaned Si substrates respectively. Figure 2 provides evidence for the morphological behavior outlined in Figure 1 above. One

observes quite contrasting film behavior that reinforces the complex interactions of PS and PVP blocks with the deposition solvent. Firstly, PSPVP3 films cast from toluene show a self-assembled surface micellar structure (Figure 2a) as expected from the cloudy solutions seen after dissolution (see inset of Figure 2a). This was confirmed by DLS measurements showing the presence of large micellar structures in toluene with a hydrodynamic diameter, $D_H \approx 450$ nm, as shown in Figure 2d. In contrast, when using more PVP selective solvents like chloroform or PGMEA, no hints of micellar structures were observed by DLS with only the presence of PSPVP unimers in solution (see Figure 2e and f). Accordingly, line-space patterns evolve in as-cast films (see Figure 2b and c). However, it must be noted that one does observe a dramatic difference in the ordering of the self-assembled structure when using PGMEA, a low vapor pressure solvent, in comparison to chloroform. Such behavior demonstrates how kinetic barriers associated to the self-assembly process and polymer chain mobility during the spin-coating step significantly influence the resulting self-assembled structure.[41] Based on the initial results for PSPVP3, this prompted us to further evaluate different surface chemistry treatments and polymer-solvent interactions for two other lamellar PSPVP molecular weight systems, *i.e.* total $M_n \sim 50$ kg mol^{-1} (PSPVP1) and total $M_n \sim 199$ kg mol^{-1} (PSPVP2). The purpose for this was twofold. Firstly, reproducing ordered out-of-plane lamellar features in a range of PSPVP BCP molecular weights would prove conclusively that the innate characteristics of PGMEA as a deposition solvent are indeed critical in the self-assembly and enhanced plasticization of polymer chains. Secondly, we also wanted to define long-range ordered patterns of the UHMW PSPVP3 in a simple and rapid manner for potential optical applications where large periodic structures are needed.

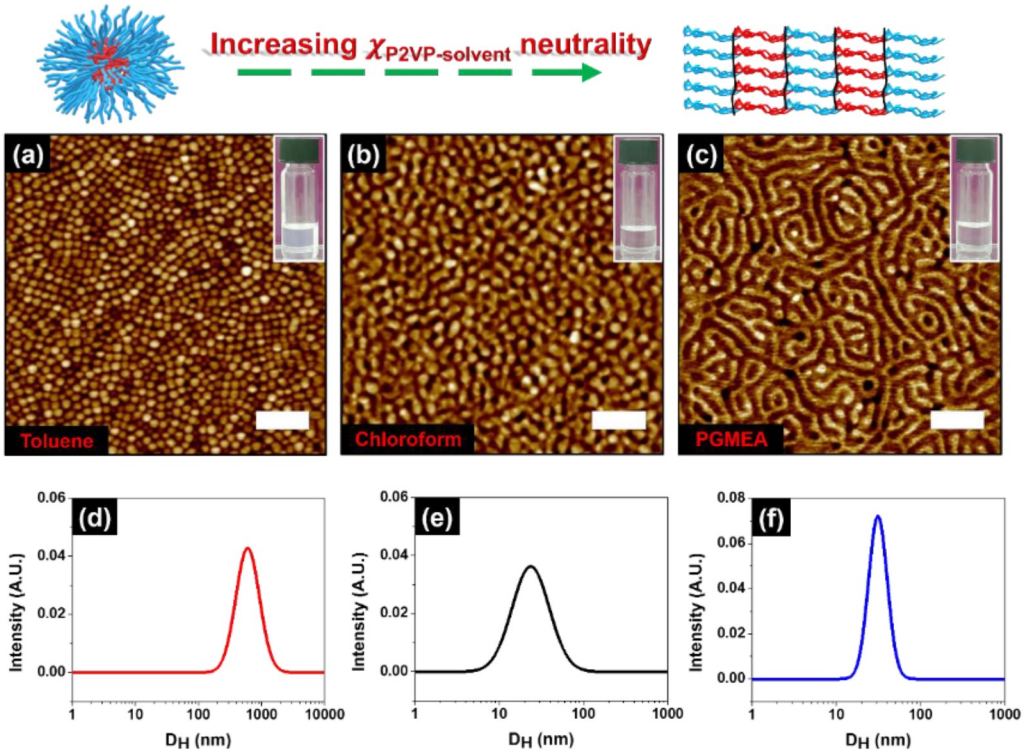

Figure 2. AFM height images of lamellar PS-*b*-P2VP (213 kg mol^{-1} – 215 kg mol^{-1}, PSPVP3) BCP films on UV/O_3 cleaned Si cast from **(a)** toluene, **(b)** chloroform, and **(c)** PGMEA. Scale bars represent 500 nm. Insets in each image show respective solutions with slightly opaque solution for toluene and transparent solutions for both chloroform and PGMEA. Diameter distributions accessed by dynamic light scattering for corresponding toluene, chloroform and PGMEA solutions are shown in **(d)-(f)**.

Polymer-solvent interactions and PSPVP film formation on PS-*stat*-PMMA treated surfaces. Figure 3 displays AFM (Figure 3 a-c), SEM (Figure 3 d-f) and GISAXS (Figure 3 g-i) data of PSPVP1, PSPVP2, and PSPVP3 films directly after spin coating from PGMEA. Films were deposited from PGMEA solutions on Si surfaces modified with a PS-*stat*-PMMA polymer (surface free energy ≈ 43 mN/m, see contact angle measurements and XPS in SI Figure S1 and S2). Note that we previously reported the use of PGMEA with respect to PSPVP2.[42] PGMEA is an industry accepted solvent since it is non-toxic, and is therefore very appealing for use with BCP lithography and thin film deposition in general.[43]

In the present study, we observed that well-defined PS and P2VP microdomains are formed for PSPVP1 and PSPVP2 in as-cast form when deposited from PGMEA only on PS-*stat*-PMMA surfaces. For comparison, corresponding data of PSPVP1-3 deposited from PGMEA on both solvent cleaned only Si and UV/O_3 cleaned Si surfaces is shown in SI Figure S4. The formation of out-of-plane PSPVP 1 and PSPVP 2 lamellar structures is displayed in respective AFM height images (Figure 3a and b) and top-down SEM characterization (see Figure 3d and e). Moreover, GISAXS analysis of the as-cast PSPVP1 and PSPVP2 films reveals the out-of-plane orientation of the lamellar features as indicated by the Bragg rods extending along α_f in Figure 3g and h. Periods were calculated from AFM, SEM and GISAXS data as ≈ 30 nm (PSPVP1) and ≈ 64 nm (PSPVP2) respectively. Although we observed self-assembled patterns for PSPVP3 (Figure 3c and f), the resulting structure is ill-defined. This is further confirmed on the GISAXS pattern below (see Figure 3f) in which only a faint first order Bragg rod is retrieved at $q_y = 0.055$ nm^{-1} (period ≈ 114 nm) and no higher order Bragg rods are visible (line cuts and discussion of GISAXS data in Figure 3 is presented in SI Figure S5).

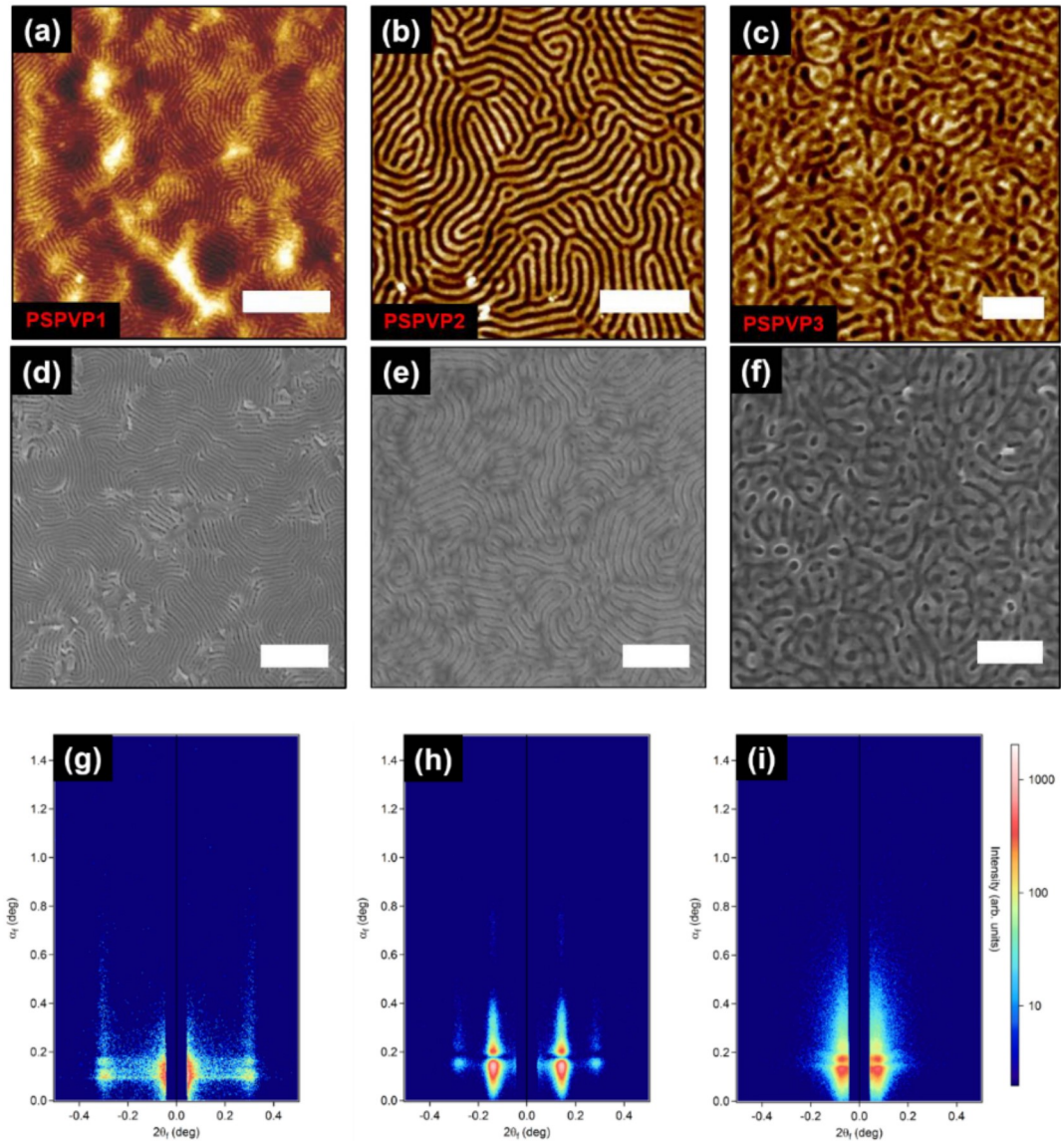

Figure 3. AFM height images of as-cast self-assembled lamellar PS-*b*-P2VP BCP films on Si with molecular weights of **(a)** 25 kg mol^{-1} – 25 kg mol^{-1} (PSPVP1), **(b)** 102 kg mol^{-1} – 97 kg mol^{-1} (PSPVP2) **(c)** 213 kg mol^{-1} – 215 kg mol^{-1} (PSPVP3). **(d)-(f)** Corresponding SEM images of (a)-(c). Note that films were swollen in ethanol for 10 minutes to provide sufficient contrast for SEM characterization. Scale bars for all AFM and SEM images are 500 nm respectively. **(g)-(i)** Corresponding GISAXS data for PSPVP1, PSPVP2, and PSPVP3 as-cast films.

In an effort to emphasize the rationale for the impressive capacity of lamellar PSPVP systems to self-assemble when simply deposited from PGMEA, we next discuss our

observation of films deposited from toluene and chloroform as casting solvents for PSPVP1-3. The following remarks reinforce the ability that PGMEA has to plasticize PSPVP polymer chains. Indeed, we assert that a highly swollen film state during the drying of PGMEA allows the polymer chains sufficient time to detangle. Respective polymer-solvent interaction parameters calculated using Hansen solubility values (as detailed in reference[44]) for PS, P2VP, toluene, chloroform and PGMEA are displayed in Table 2 below. Toluene and chloroform are commonly used solvents for both PSPVP BCP deposition and SVA.[45,46,47,48,49] However, toluene (vapor pressure = 3.78 kPa @ 25°C) and chloroform (vapor pressure = 25.12 kPa @ 25°C) are volatile solvents (although chloroform is markedly more volatile than toluene) in comparison to PGMEA (vapor pressure = 0.50 kPa @ 25°C) and can therefore lead to film instability or kinetically trapped micellar structures. As discussed earlier, this is especially true with respect to films cast from toluene since toluene is a PS favorable solvent. For example, $\chi_{PVP\text{-}PGMEA}$ is 0.32, indicating that PGMEA is a good solvent for PVP which contrasts significantly to toluene where $\chi_{PVP\text{-}Toluene}$ = 1.46.

Table 2. Dispersive, polar and hydrogen bonding values for PSPVP BCPs and solvents studied here.

Polymer or Solvent	δ_d (MPa$^{1/2}$)	δ_p (MPa$^{1/2}$)	δ_h (MPa$^{1/2}$)	V (μm^3 /mol)[a]	Vapor pressure (kPa)	$\chi_{polymer\text{-}Toluene}$[b]	$\chi_{polymer\text{-}Chloroform}$[b]	$\chi_{polymer\text{-}PGMEA}$[b]
Toluene	18.0	1.4	2.0	106.8	3.78	-	-	-
Chloroform	17.8	3.1	5.7	80.7	25.12	-	-	-
PGMEA	16.1	6.1	6.6	137.1	0.50	-	-	-
Poly(styrene)	18.7	5.9	3.5	115	-	0.27	0.15	0.46
Poly(2-vinylpyridine)	16.4	7.1	11.6	108	-	1.46	0.55	0.32

[a] Vapor pressure is at 25°C. [b] Values of χ parameters were estimated at 25°C using $\chi_{AB} = \frac{V}{RT}\left((\delta_{dA} - \delta_{dB})^2 + 0.25\left(\delta_{pA} - \delta_{pB}\right)^2 + 0.25(\delta_{hA} - \delta_{hB})^2\right)$.

The SI discusses the drastic difference in film formation, thickness, and surface coverage observed experimentally on different surface treatments for PSPVP1-3 cast from toluene (SI Figure S6) and chloroform (SI Figure S7) solutions. After our comprehensive study of polymer-solvent interaction values for PSPVP1-3, as well as considering substrate surface chemistry-PSPVP pattern formation, we believe the low volatility of PGMEA combined with the balanced interaction of PS and P2VP block with PGMEA allows more stable films to form and prevents thin film rupture upon deposition as can occur with volatile solvents like toluene and chloroform. Further investigation is needed using in-situ GISAXS, for example, and may lead to a more comprehensive view on the kinetics of the systems during deposition.

Enhancing UHMW PSPVP Pattern Formation. Despite forming perpendicular PSPVP3 patterns in as-cast form (see Figure 2c, 3c and f), we further investigated conditions to enhance correlation lengths to acceptable standards (> 1 μm). Although PS-*stat*-PMMA treated surfaces can be used for PSPVP3 pattern formation, we devised after several baseline experiments that PS-*stat*-P2VP modified surfaces (surface free energy of PS-*stat*-P2VP was ≈ 47 mN/m, see contact angle measurements and XPS in SI Figure S8 and S9) were more favorable for forming well-ordered features after solvent vapor annealing. **Figure 4a** displays an AFM height image of a 5 x 5 μm area in which excellent PSPVP3 patterns are evident after processing on PS-*stat*-P2VP treated surfaces and solvent vapor annealing with PGMEA/$CHCl_3$ for 1 hr at room temperature (20°C). Experiments on unmodified Si surfaces showed large area dewetting (see SI Figure 10) and no evidence of microphase separated patterns emphasizing the need for the PS-*stat*-P2VP underlayer. Moreover, solvent vapor annealing of PSPVP3 on PS-*stat*-PMMA under PGMEA, $CHCl_3$ or PGMEA/$CHCl_3$ solvent atmospheres (see SI Figure 11) did not

produce ordered microdomains as observed on PS-*stat*-P2VP treated surfaces. Figure 4b shows the corresponding top-down SEM image of PSPVP3 films where well defined areas are evident. From our experimental observations, we believe the combination of a PGMEA and $CHCl_3$ atmosphere provides sufficient swelling and enhanced chain mobility for both PS and P2VP. We infer this given that the value for $\chi_{PVP\text{-}PGMEA}$ is 0.32 and $\chi_{PS\text{-}CHCl3}$ is 0.15 (See values in Table 2 above). Additionally, we carried out GISAXS analysis to characterize the large scale ordering of the films developed, and Figure 4c exhibits Bragg rods characteristic of perpendicular lamella formation. The periodicity calculated from the GISAXS pattern is ≈ 111 nm. Moreover, the corresponding line-cut along q_y integrated around the Yoneda band (Figure 4d) from the GISAXS data validates the assertion of perpendicular PSPVP formation as a first-order peak at 0.057 nm^{-1} and higher-order peaks located at $q/q^* = 1, 2, 3$ are observed.

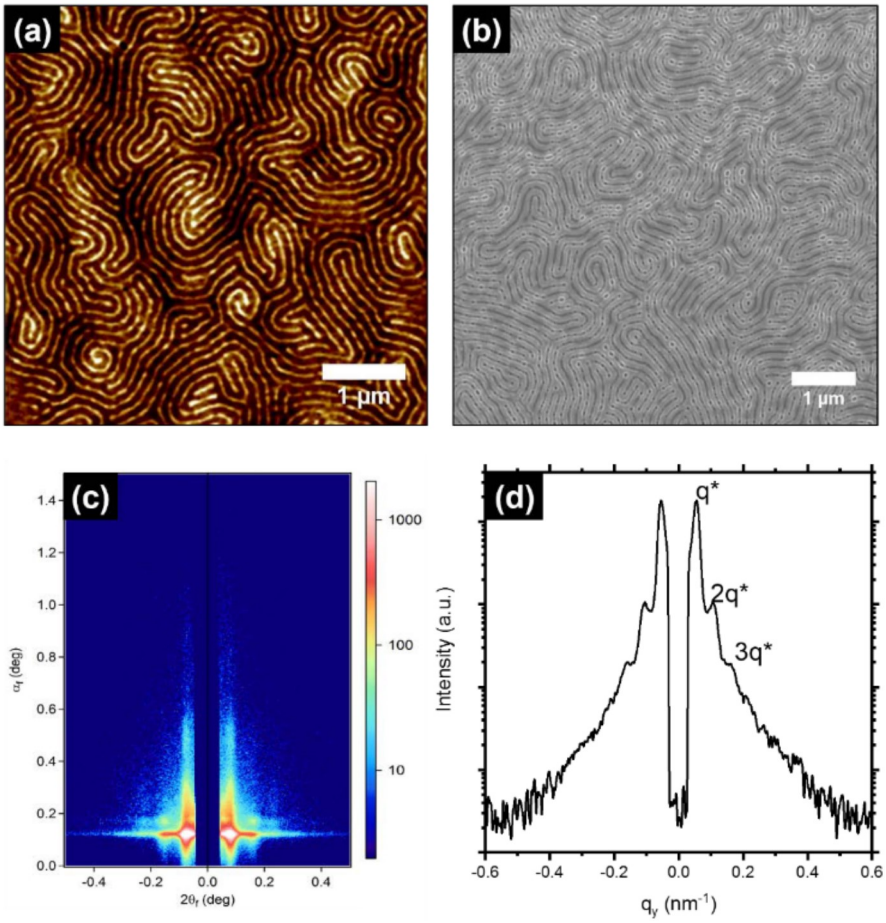

Figure 4. (a) AFM height image (5 x 5 μm area) of well-ordered PSPVP3 BCP line structures (period ≈ 111 nm) after 1hr SVA. **(b)** Corresponding top-down SEM image of PSPVP3 structures. **(c)** GISAXS profile of well-ordered PSPVP3 structure. Films were swollen in ethanol for 10 minutes to provide sufficient contrast for SEM characterization and GISAXS. **(d)** In-plane scattering profile corresponding to a horizontal cut for PSPVP3 after SVA.

Metallic and dielectric fabrication from UHMW PSPVP templates. As an exemplar, we used the ultra large period PSPVP3 templates to fabricate gold (Au) and alumina (AlO_x) nanostructures as displayed in **Figure 5a-d**. In a first instance, we have developed Au nanofeatures using *aq.* $HAuCl_4$ solutions. Varying concentrations (1-10 *wt.* %) were spin coated on the self-assembled PSPVP3 patterns, and followed by 60 secs of O_2 plasma treatment. O_2 plasma is used to achieve Au^0 chemical state as determined by XPS (see SI Figure S12) of deposited $HAuCl_4$ precursors. Au spheres were initally observed from 1 wt. % $HAuCl_4$ solutions as shown in SI Figure S13. Rod-like Au nanostructures (Figure 5a) and Au nanowires (Figure 5b) were developed with respect to $HAuCl_4$ precursor concentration, *i.e.* 5 wt. % vs 10 wt. %. Variable angle spectroscopic analysis is shown and discussed in SI Figure Sxx confirming the plasmon resonance (LSPR) of the Au arrays created from the P2VP domains.

In a second demonstration, we exemplify the ability to pattern the reactive P2VP microdomains in PSPVP3 using sequential infiltration synthesis (SIS) to write dense features of AlO_x nanowires (Figure 5c and d). SIS is an atomic layer deposition (ALD) derived process, that infiltrates selective polymer block domains to allow isolated feature formation for various applications. For example, one can create pattern transfer hardmasks for nanooelectronic circuity,[50] porous inorganic antireflective coatings,[51] and vapor sensors.[52] In our experiments, after SIS, an O_2 plasma treatment was used to remove the PS matrix revealing distinct AlOx nanowires. 3 SIS cycles proved sufficient for

formation of dense AlOx features as shown in Figure 5c with feature sizes of 63 nm. Additionally, 5 SIS cycles increased the AlOx feature sizes to 73 nm. This is a valulable asset for lithogrpahic patterning and shows the potential to further dial in specific feature sizes with SIS, an industry compatible technology.

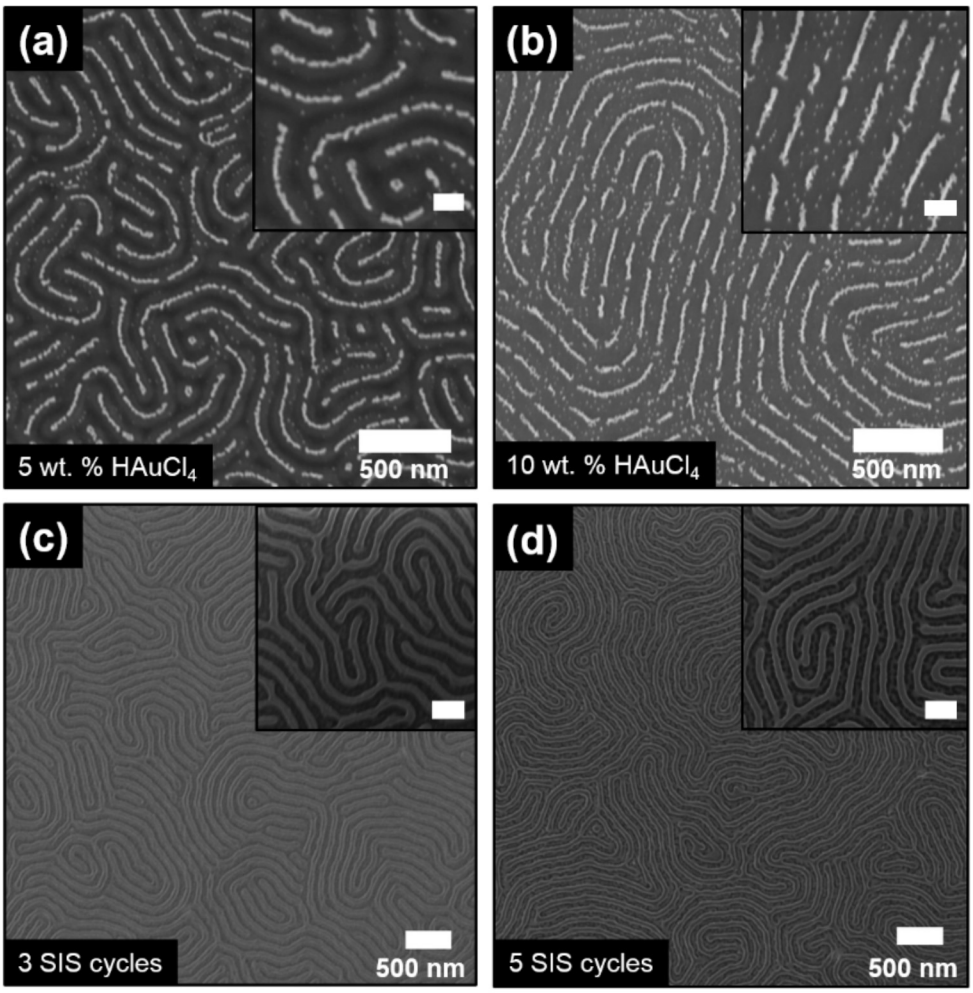

Figure 5. Large period metallic and dielectric feature formation. (a,b) Top-down SEM images showing Au metallic features from 5 wt. % and 10 wt. % $HAuCl_4$ solutions deposited on PSPVP3 templates and treated with O_2 plasma. Insets show high-resolution images of defined Au features, scale bars are 100 nm. **(c,d)** Top-down SEM images showing AlO_x feature formation after SIS treatment for 3 cycles and 5 cycles respectively. Insets show high-resolution images of AlO_x features, scale bars are 200 nm. Periods in all images are ≈ 110 nm.

In this latter section, we have showcased the ability of a large period BCP system to generate isolated metallic and dielectric features. The process is advantageous over traditional top-down lithography (*e.g.* ultraviolet lithography, e-beam lithography, nanoimprint lithography) and other wet chemistry approaches including ease of processing, rapid fabrication and material sets available to pattern in the initial template (both metallic and dielectric). The fabrication strategy described here to produce ultra-large periodic features may be useful for flat optics integration where compact and ultra-thin layers are required. [53,54]

CONCLUSIONS

Despite the long history of PSPVP BCP thin film reports, our study shows that understanding and analysis of deposition processes greatly influence the ability to pattern well-ordered lamellar PSPVP BCPs. While mixed solvents are commonly used for dissolving PSPVP *e.g.* toluene/THF is used to avoid micellization,[55,56] we have shown that PGMEA is an ideal solvent to pattern PSPVP lamellar features and enhance polymer chain mobility of an UHMW PS-*b*-P2VP. Vertical ordering of PSPVP lamellae was verified via top-down (AFM and SEM imaging) and in-film techniques (GISAXS data) and shows a scalable and industrial compatible process across three PSPVP molecular weights. In particular, we have elucidated the optimized process window for ultra large PS-*b*-P2VP periods at 111 nm. Additionally, we have shown an early example towards large period Au and AlO_x structures that are of interest for future large scale integration. In summary, our demonstration proves that UHMW linear di-BCP materials have the potential to self-assemble with excellent registry over large scale areas in 1 hr. We stress that more studies are required to extend to even higher BCP period values, *e.g.* > 200 nm, akin to optical waveguides, that are truly applicable to visible and near-infrared light applications. Future work will look toward exploring larger lamellar molecular weight

BCPs and to develop more dense metallic or dielectric features (in both pattern diameter and height).

■ AUTHOR INFORMATION

* Corresponding Authors:

C.C. - cian.a.cummins@gmail.com

V.P. - virginie.ponsinet@u-bordeaux.fr

G.F. - guillaume.fleury@u-bordeaux.fr

ORCID

C.C. 0000-0001-6338-3991

G.H. 0000-0002-7377-6040

G.F. 0000-0003-0779-191X

V.P. 0000-0002-0301-5932

Notes

The authors declare no competing financial interest.

■ ACKNOWLEDGMENTS

The authors are sincerely grateful for financial support from the University of Bordeaux and the LabEx AMADEus (ANR-10-LABEX-0042-AMADEUS). This work was performed within the framework of the Equipex ELORPrintTec ANR-10-EQPX-28-01 with the help of the French state's Initiative d'Excellence IdEx ANR-10-IDEX-003-02. The authors also thank the LCPO support staff: Aude Manson, Melanie Bousquet, Ellena Karnezis, and Gilles Pecastaings for their help.

REFERENCES

1. Bates, F. S.; Fredrickson, G. H., Block copolymers - Designer soft materials. *Physics Today* **1999,** *52* (2), 32-38.

2. Morris, M. A., Directed self-assembly of block copolymers for nanocircuitry fabrication. *Microelectronic Engineering* **2015,** *132*, 207-217.
3. Bates, F. S.; Hillmyer, M. A.; Lodge, T. P.; Bates, C. M.; Delaney, K. T.; Fredrickson, G. H., Multiblock Polymers: Panacea or Pandora's Box? *Science* **2012,** *336* (6080), 434-440.
4. Nunes, S. P.; Culfaz-Emecen, P. Z.; Ramon, G. Z.; Visser, T.; Koops, G. H.; Jin, W.; Ulbricht, M., Thinking the future of membranes: Perspectives for advanced and new membrane materials and manufacturing processes. *Journal of Membrane Science* **2019**, 117761.
5. Kim, J. H.; Jin, H. M.; Yang, G. G.; Han, K. H.; Yun, T.; Shin, J. Y.; Jeong, S.-J.; Kim, S. O., Smart Nanostructured Materials based on Self-Assembly of Block Copolymers. *Advanced Functional Materials* **2019,** *n/a* (n/a), 1902049.
6. Wang, X.; Ehrhardt, K.; Tallet, C. m.; Warenghem, M.; Baron, A.; Aradian, A.; Kildemo, M.; Ponsinet, V., Hyperbolic-by-design self-assembled metamaterial based on block copolymers lamellar phases. *Optics and Laser Technology* **2017,** *88*, 85-95.
7. Cummins, C.; Morris, M. A., Using block copolymers as infiltration sites for development of future nanoelectronic devices: Achievements, barriers, and opportunities. *Microelectronic Engineering* **2018,** *195*, 74-85.
8. Alvarez-Fernandez, A.; Fleury, G.; Ponsinet, V.; Walmsness, P. M.; Kildemo, M., Formation and optical response of self-assembled gold nanoparticle lattices on oxidized silicon synthesized using block copolymers. *Journal of Vacuum Science & Technology B* **2020,** *38* (1), 013601.
9. Agrahari, V.; Agrahari, V., Advances and applications of block-copolymer-based nanoformulations. *Drug Discovery Today* **2018,** *23* (5), 1139-1151.
10. Schacher, F. H.; Rupar, P. A.; Manners, I., Functional block copolymers: Nanostructured materials with emerging applications. *Angewandte Chemie - International Edition* **2012,** *51* (32), 7898-7921.
11. Ross, C. A.; Berggren, K. K.; Cheng, J. Y.; Jung, Y. S.; Chang, J.-B., Three-Dimensional Nanofabrication by Block Copolymer Self-Assembly. *Advanced Materials* **2014,** *26* (25), 4386-4396.
12. Gabinet, U. R.; Osuji, C. O., Optical materials and metamaterials from nanostructured soft matter. *Nano Research* **2019,** *12* (9), 2172-2183.
13. Hu, H.; Gopinadhan, M.; Osuji, C. O., Directed self-assembly of block copolymers: a tutorial review of strategies for enabling nanotechnology with soft matter. *Soft Matter* **2014,** *10* (22), 3867-3889.
14. Cummins, C.; Lundy, R.; Walsh, J. J.; Ponsinet, V.; Fleury, G.; Morris, M. A., Enabling future nanomanufacturing through block copolymer self-assembly: A review. *Nano Today* **2020,** *35*, 100936.
15. Cummins, C.; Ghoshal, T.; Holmes, J. D.; Morris, M. A., Strategies for Inorganic Incorporation using Neat Block Copolymer Thin Films for Etch Mask Function and Nanotechnological Application. *Advanced materials (Deerfield Beach, Fla.)* **2016,** *28* (27), 5586-618.
16. Bas, S. Z.; Cummins, C.; Borah, D.; Ozmen, M.; Morris, M. A., Electrochemical Sensing of Hydrogen Peroxide Using Block Copolymer Templated Iron Oxide Nanopatterns. *Analytical Chemistry* **2018,** *90* (2), 1122-1128.
17. Shin, D. O.; Mun, J. H.; Hwang, G.-T.; Yoon, J. M.; Kim, J. Y.; Yun, J. M.; Yang, Y.-B.; Oh, Y.; Lee, J. Y.; Shin, J.; Lee, K. J.; Park, S.; Kim, J. U.; Kim, S. O., Multicomponent Nanopatterns by Directed Block Copolymer Self-Assembly. *ACS Nano* **2013,** *7* (10), 8899-8907.
18. Cummins, C.; Bell, A. P.; Morris, M. A., Creating Active Device Materials for Nanoelectronics Using Block Copolymer Lithography. *Nanomaterials (Basel, Switzerland)* **2017,** *7* (10), 304.
19. Sarkar, A.; Jeon, N. J.; Noh, J. H.; Seok, S. I., Well-Organized Mesoporous TiO2 Photoelectrodes by Block Copolymer-Induced Sol–Gel Assembly for Inorganic–Organic Hybrid Perovskite Solar Cells. *The Journal of Physical Chemistry C* **2014,** *118* (30), 16688-16693.

20. Monticone, F.; Alù, A., Metamaterial, plasmonic and nanophotonic devices. *Reports on Progress in Physics* **2017,** *80* (3), 036401.
21. Yu, N.; Capasso, F., Flat optics with designer metasurfaces. *Nat Mater* **2014,** *13* (2), 139-50.
22. Bukhari, S. S.; Vardaxoglou, J.; Whittow, W., A Metasurfaces Review: Definitions and Applications. *Applied Sciences* **2019,** *9* (13).
23. Verduzco, R.; Li, X.; Pesek, S. L.; Stein, G. E., Structure, function, self-assembly, and applications of bottlebrush copolymers. *Chemical Society Reviews* **2015,** *44* (8), 2405-2420.
24. Hong, S. W.; Gu, W.; Huh, J.; Sveinbjornsson, B. R.; Jeong, G.; Grubbs, R. H.; Russell, T. P., On the Self-Assembly of Brush Block Copolymers in Thin Films. *ACS Nano* **2013,** *7* (11), 9684-9692.
25. Yang, Q.; Loos, K., Perpendicular Structure Formation of Block Copolymer Thin Films during Thermal Solvent Vapor Annealing: Solvent and Thickness Effects. *Polymers* **2017,** *9* (10).
26. Kim, E.; Ahn, H.; Park, S.; Lee, H.; Lee, M.; Lee, S.; Kim, T.; Kwak, E.-A.; Lee, J. H.; Lei, X.; Huh, J.; Bang, J.; Lee, B.; Ryu, D. Y., Directed Assembly of High Molecular Weight Block Copolymers: Highly Ordered Line Patterns of Perpendicularly Oriented Lamellae with Large Periods. *ACS Nano* **2013,** *7* (3), 1952-1960.
27. Doerk, G. S.; Li, R.; Fukuto, M.; Yager, K. G., Wet Brush Homopolymers as "Smart Solvents" for Rapid, Large Period Block Copolymer Thin Film Self-Assembly. *Macromolecules* **2020,** *53* (3), 1098-1113.
28. Takano, K.; Nyu, T.; Maekawa, T.; Seki, T.; Nakatani, R.; Komamura, T.; Hayakawa, T.; Hayashi, T., Real-time and in situ observation of structural evolution of giant block copolymer thin film under solvent vapor annealing by atomic force microscopy. *RSC Advances* **2020,** *10* (1), 70-75.
29. Rasappa, S.; Hulkkonen, H.; Schulte, L.; Ndoni, S.; Reuna, J.; Salminen, T.; Niemi, T., High molecular weight block copolymer lithography for nanofabrication of hard mask and photonic nanostructures. *Journal of Colloid and Interface Science* **2019,** *534*, 420-429.
30. Mokarian-Tabari, P.; Senthamaraikannan, R.; Glynn, C.; Collins, T. W.; Cummins, C.; Nugent, D.; O'Dwyer, C.; Morris, M. A., Large Block Copolymer Self-Assembly for Fabrication of Subwavelength Nanostructures for Applications in Optics. *Nano Letters* **2017,** *17* (5), 2973-2978.
31. Wang, H. S.; Kim, K. H.; Bang, J., Thermal Approaches to Perpendicular Block Copolymer Microdomains in Thin Films: A Review and Appraisal. *Macromolecular Rapid Communications* **2019,** *40* (4), 1800728.
32. Lundy, R.; Yadav, P.; Selkirk, A.; Mullen, E.; Ghoshal, T.; Cummins, C.; Morris, M. A., Optimizing Polymer Brush Coverage To Develop Highly Coherent Sub-5 nm Oxide Films by Ion Inclusion. *Chemistry of Materials* **2019,** *31* (22), 9338-9345.
33. Sinturel, C.; Vayer, M.; Morris, M.; Hillmyer, M. A., Solvent Vapor Annealing of Block Polymer Thin Films. *Macromolecules* **2013,** *46* (14), 5399-5415.
34. Jiang, Z., GIXSGUI: a MATLAB toolbox for grazing-incidence X-ray scattering data visualization and reduction, and indexing of buried three-dimensional periodic nanostructured films. *Journal of Applied Crystallography* **2015,** *48* (3), 917-926.
35. Dai, K. H.; Kramer, E. J., Determining the temperature-dependent Flory interaction parameter for strongly immiscible polymers from block copolymer segregation measurements. *Polymer* **1994,** *35* (1), 157-161.
36. Lu, J. Q.; Yi, S. S., Uniformly Sized Gold Nanoparticles Derived from PS-b-P2VP Block Copolymer Templates for the Controllable Synthesis of Si Nanowires. *Langmuir* **2006,** *22* (9), 3951-3954.
37. Lu, J. Q., Nanocatalysts with tunable properties derived from polystyrene-*b*-poly(vinyl pyridine) block copolymer templates for achieving controllable carbon nanotube synthesis. *Journal of Physical Chemistry C* **2008,** *112* (28), 10344-10351.
38. Yoo, H.; Park, S., The fabrication of highly ordered block copolymer micellar arrays: control of the separation distances of silicon oxide dots. *Nanotechnology* **2010,** *21* (24).

39. Park, S.; Wang, J.-Y.; Kim, B.; Chen, W.; Russell, T. P., Solvent-Induced Transition from Micelles in Solution to Cylindrical Microdomains in Diblock Copolymer Thin Films. *Macromolecules* **2007,** *40* (25), 9059-9063.
40. Park, S.; Kim, B.; Xu, J.; Hofmann, T.; Ocko, B. M.; Russell, T. P., Lateral Ordering of Cylindrical Microdomains Under Solvent Vapor. *Macromolecules* **2009,** *42* (4), 1278-1284.
41. Vayer, M.; Vital, A.; Sinturel, C., New insights into polymer-solvent affinity in thin films. *European Polymer Journal* **2017,** *93*, 132-139.
42. Alvarez-Fernandez, A.; Aissou, K.; Pécastaings, G.; Hadziioannou, G.; Fleury, G.; Ponsinet, V., High refractive index in low metal content nanoplasmonic surfaces from self-assembled block copolymer thin films. *Nanoscale Advances* **2019,** *1* (2), 849-857.
43. Böhme, S.; Girardot, C.; Garnier, J.; Arias-Zapata, J.; Arnaud, S.; Tiron, R.; Marconot, O.; Buttard, D.; Zelsmann, M. In *A route for industry compatible directed self-assembly of high-chi PS-PDMS block copolymers*, 2016; pp 97771W-97771W-10.
44. Hansen, C. M., Hansen solubility parameters: a user's handbook. *CRC Press* **2007**.
45. Park, S.; Kim, B.; Cirpan, A.; Russell, T. P., Preparation of Metallic Line Patterns from Functional Block Copolymers. *Small* **2009,** *5* (11), 1343-1348.
46. Ogawa, H.; Takenaka, M.; Miyazaki, T.; Fujiwara, A.; Lee, B.; Shimokita, K.; Nishibori, E.; Takata, M., Direct Observation on Spin-Coating Process of PS-b-P2VP Thin Films. *Macromolecules* **2016,** *49* (9), 3471-3477.
47. Ogawa, H.; Takenaka, M.; Miyazaki, T.; Kabe, T.; Kanaya, T., Order–Order Transition Processes of Thin-Film Symmetric and Asymmetric PS-b-P2VP during Spin Coating. *Macromolecules* **2018,** *51* (23), 10040-10051.
48. Yin, J.; Yao, X.; Liou, J.-Y.; Sun, W.; Sun, Y.-S.; Wang, Y., Membranes with Highly Ordered Straight Nanopores by Selective Swelling of Fast Perpendicularly Aligned Block Copolymers. *ACS Nano* **2013,** *7* (11), 9961-9974.
49. Cheng, X.; Böker, A.; Tsarkova, L., Temperature-Controlled Solvent Vapor Annealing of Thin Block Copolymer Films. *Polymers* **2019,** *11* (8), 1312.
50. Cummins, C.; Mantione, D.; Cruciani, F.; Pino, G.; Demazy, N.; Shi, Y.; Portale, G.; Hadziioannou, G.; Fleury, G., Rapid Self-Assembly and Sequential Infiltration Synthesis of High χ Fluorine-Containing Block Copolymers. *Macromolecules* **2020**.
51. Berman, D.; Guha, S.; Lee, B.; Elam, J. W.; Darling, S. B.; Shevchenko, E. V., Sequential Infiltration Synthesis for the Design of Low Refractive Index Surface Coatings with Controllable Thickness. *ACS Nano* **2017,** *11* (3), 2521-2530.
52. Greil, S.; Rahman, A.; Liu, M.; Black, C. T., Gas Transport Selectivity of Ultrathin, Nanoporous, Inorganic Membranes Made from Block Copolymer Templates. *Chemistry of Materials* **2017,** *29* (21), 9572-9578.
53. Chang, S.; Guo, X.; Ni, X., Optical Metasurfaces: Progress and Applications. *Annual Review of Materials Research* **2018,** *48* (1), 279-302.
54. Kang, L.; Jenkins, R. P.; Werner, D. H., Recent Progress in Active Optical Metasurfaces. *Advanced Optical Materials* **2019,** *7* (14), 1801813.
55. Ghoshal, T.; Chaudhari, A.; Cummins, C.; Shaw, M. T.; Holmes, J. D.; Morris, M. A., Morphological evolution of lamellar forming polystyrene-block-poly(4-vinylpyridine) copolymers under solvent annealing. *Soft Matter* **2016**.
56. Park, S.; Kim, B.; Wang, J. Y.; Russell, T. P., Fabrication of Highly Ordered Silicon Oxide Dots and Stripes from Block Copolymer Thin Films. *Advanced Materials* **2008,** *20* (4), 681-685.

For table of contents (TOC) use only: